Brodogradnja Volume 77 Number 2 (2026) 77208

University of Zagreb
Faculty of Mechanical
Engineering and Naval
Architecture

journal homepage: www.brodogradnja.fsb.hr

Brodogradnja

An International Journal of Naval Architecture and
Ocean Engineering for Research and Development

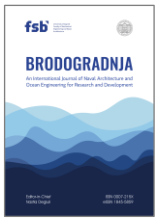

Numerical study on the influence of localized damage effect of explosives on steel plate structure damage under underwater contact explosions

Guangliang Li[1*], *Dongyan Shi*[2], *Lifu Wang*[3], *Kun Zhao*[2]

[1] *College of Mechanical Engineering, Hunan University of Technology, Hunan 412000, China*
[2] *College of Mechanical and Electrical Engineering, Harbin Engineering University, Harbin 150001, China*
[3] *College of Mechanical and Electrical Engineering, Northeast Forestry University, Harbin 150001, China*

ARTICLE INFO

Keywords:
Underwater contact explosion
Steel plate
Structure damage
Localized damage effect of explosive

ABSTRACT

This study investigates the fluid-structure interaction dynamics induced by underwater explosive, focusing on the impact of localized damage effects of explosive on the transient interaction between plate structures. To accurately characterize this localized effect, numerical experiments were conducted on the damage to a steel plate subjected to underwater explosive shock under various charge and explosion distance conditions. Results indicate that the diameter of plate perforations caused by contact explosions is smaller than that under conditions with a certain explosion distance. By establishing the relationship between relative explosion distance and plate perforation diameter, the optimal range for the localized damage effect of explosive is determined to be a relative explosion distance of 1.1–2. Furthermore, the relationship between the impact factor and the structural dimensionless factor, established based on the plate damage results, conforms to a quadratic function dependency. This relationship characterizes the role of the local effect of the munition in the inherent local damage mechanism of the target structure. These research findings provide empirical guidance for enhancing the lethality of underwater weapons and optimizing the efficiency of underwater mining, underwater de-icing, and other engineering operations.

1. Introduction

As a complex multi-physical field coupling phenomenon, underwater explosion is widely present in the fields of national defense security and civil engineering. At the national defense level, the assessment of the lethality of underwater weapons and the design of anti-explosion protection for equipment such as warships and submarines all rely on the damage mechanism of underwater explosion to structures as the core basis [1-3]. In the civil field, the optimization of dredging blocked dams efficiency in underwater mining and the safety guarantee of underwater de-icing operations in polar waterways also depend on the accurate grasp of the laws of underwater explosion energy transfer and structural response [4-9]. However, due to the complexity of explosive energy release, shock wave propagation, and fluid-structure interaction (i.e., fluid-structure interaction dynamics) during the underwater explosion process, the correlation mechanism between

* Corresponding author.
E-mail address: 14550@hut.edu.cn

https://doi.org/10.21278/brod77208
Received 23 March 2025; Received in revised form 14 September 2025; Accepted 17 November 2025
Available online 26 November 2025
ISSN 0007-215X; eISSN 1845-5859

the local damage effect of ammunition and the transient response of structures has not been fully clarified. In particular, the quantitative impact of ammunition parameters on the damage effect of target structures still lacks systematic theoretical support and experimental verification, which greatly limits the engineering application efficiency of underwater explosion-related technologies.

Most existing research focused on ship components, such as stiffened plates and hull girders, to evaluate their deformation, failure mechanisms, and structural integrity [10], with insufficient targeted analysis of the local damage effect of explosives. For example, He et al. [11] conducted near-field underwater explosion tests on full-scale warships and studied the dynamic response process of the structures. Subsequently, they further employed machine learning methods to predict the structural response under underwater explosions and developed a method for rapidly predicting the deformation of ship structures subjected to underwater explosions [12]. Madsen et al. [13] conducted underwater explosion experiments on flat plates with different thicknesses and obtained the interaction relationships between different load characteristics and the structure. Cheng et al. [14] conducted experimental studies on complex multi-compartment structures, revealing the cumulative damage mechanism of structures under the action of repeated underwater explosions and evaluating the influence of explosion distance on damage characteristics. These studies have made significant contributions to the theoretical development of underwater explosion load characteristics and structural responses. However, they fail to provide accurate thresholds for the optimization of explosive action parameters.

In the study of actual underwater explosions using model experiments, similar laws are often explored through impact factors and structural nondimensionalization. For example, Shi et al. [15] established a similarity transformation relationship between the strain signals of the model and the prototype based on the Hurst exponent and studied the model testing of the nonlinear impact response of ship stiffened plate structures as well as the similarity laws between the model and the actual ship. Yao et al. [16, 17] conducted research on the nonlinear similarity issue of underwater explosions and revealed the similarity mechanism of the strong nonlinear dynamic responses of ship structures under explosive impact. The quantitative models used to characterize the correlation between the local effect of ammunition and structural damage are still relatively scarce.

To address the above research gaps, this study takes the fluid-structure interaction dynamics induced by explosives in underwater explosion as the core research object and focuses on exploring the influence of the local damage effect of underwater explosion ammunition on the transient interaction of plate structures. Through conducting underwater explosion numerical experiments under different charge specifications and explosion distance conditions, the study systematically analyzes the influence law of ammunition parameters on the damage effect of flat plates (such as breach diameter). Furthermore, a correlation model between the relative explosion distance and the breach diameter of flat plates is constructed to clarify the optimal action range of the local damage effect of ammunition. At the same time, a mathematical relationship between the impact factor and the structural dimensionless factor is established to quantitatively characterize the effect of the local ammunition effect on the inherent structural damage mechanism. This study aims to fill the theoretical gap in the quantitative analysis of the local damage effect of underwater explosion and provide a scientific basis for the optimization of underwater weapon design and the parameter setting of projects such as underwater mining and de-icing, which has important theoretical value and engineering practical significance.

In addition, due to the high cost and complexity of conducting underwater explosion experiments, the use of numerical simulation methods to assist in researching issues in this field has been effectively verified [18-23]. Therefore, the experiments in this paper are mainly conducted using numerical simulation methods. Specifically, the Arbitrary Lagrangian-Eulerian (ALE) method in the LS-DYNA software is adopted.

2. Numerical theory background

2.1 Arbitrary-Lagrangian-Eulerian (ALE) method

The ALE algorithm has been developed to combine the advantages of the Lagrangian and Eulerian algorithms, which has been widely used in solving the problem of FSI [24-26]. The conservation of mass, momentum, and energy used to solve fluid flow are given in Equations (1-3) [9, 24]:

$$\frac{d\rho}{dt} = \left.\frac{\partial \rho}{\partial t}\right|_x + \boldsymbol{v}\cdot\nabla\rho = -\rho\nabla\cdot\boldsymbol{v} \tag{1}$$

$$\rho\frac{d\boldsymbol{v}}{dt} = \rho\left(\left.\frac{\partial \boldsymbol{v}}{\partial t}\right|_x + (\boldsymbol{v}\cdot\nabla)\boldsymbol{v}\right) = \nabla\cdot\boldsymbol{\sigma} + \rho\boldsymbol{b} \tag{2}$$

$$\rho\frac{dE}{dt} = \rho\left(\left.\frac{\partial e}{\partial t}\right|_x + \boldsymbol{v}\cdot\nabla E\right) = \nabla\cdot(\boldsymbol{\sigma}\cdot\boldsymbol{v}) + \boldsymbol{v}\cdot\rho\boldsymbol{b} \tag{3}$$

where ρ is mass density, x is spatial point, $\boldsymbol{v}$ is material velocity vector, $\boldsymbol{\sigma}$ denotes Cauchy stress tensors, $\boldsymbol{b}$ is specific body force vector and E is total energy. Only mechanical energies are considered in the energy equation. At the same time, the stress term in same equation can be rewritten in the form:

$$\nabla\cdot(\boldsymbol{\sigma}\cdot\boldsymbol{v}) = \frac{\partial}{\partial x_i}(\sigma_{ij}v_j) = \frac{\partial\sigma_{ij}}{\partial x_i}v_j + \sigma_{ij}\frac{\partial v_j}{\partial x_i} = (\nabla\cdot\boldsymbol{\sigma})\cdot\boldsymbol{v} + \boldsymbol{\sigma}\cdot\nabla\boldsymbol{v} \tag{4}$$

where $\nabla\boldsymbol{v}$ is the spatial velocity gradient.

2.2 Material models

2.2.1 TNT

In this paper, the JWL equation of state is used to describe the interaction between pressure, internal energy and volume of detonation product of TNT, as show Eq. (5) [8, 27]. In this numerical simulation of Ls-dyna, the "*MAT_HIGH_EXPLOSIVE_BURN" and "*EOS_JWL" are applied for TNT:

$$P = A\left(1-\frac{\omega}{R_1V}\right)e^{-R_1V} + B\left(1-\frac{\omega}{R_2V}\right)e^{-R_2V} + \frac{\omega E}{V} \tag{5}$$

where A, B, ω, R_1, R_2 are the material constants, the term A, B are the pressure coefficients, V is the specific volume of detonation products, E is the internal energy per initial volume. The material parameters are listed in Table 1.

Table 1 JWL equation of state parameters [4, 28]

ρ (kg/m^3)	A (GPa)	B (GPa)	R_1	R_2	ω	E (kJ/kg)
1630	371.2	3.23	4.15	0.95	0.3	7

2.2.2 Water and air

The Gruneisen equation of state [9, 29] is introduced to calculate the internal characteristic of water, its form determined by the state of water. The equation is as follows:

$$P=\frac{\rho_0 C^2\mu[1+(1-\frac{\gamma_0}{2})\mu-\frac{\alpha}{2}\mu^2]}{[1-(S_1-1)\mu-S_2\frac{\mu^2}{\mu+1}-S_3\frac{\mu^3}{(\mu+1)^2}]}+(\gamma_0+\alpha\mu)E^{'} \tag{6}$$

where ρ_0 is the instantaneous density, C is the intercept of the shock velocity curve, E is the internal energy per initial volume; S_1, S_2 and S_3 are the unitless coefficients of the slope of the shock velocity curve, γ_0 is the Gruneisen gamma, and α is the first-order volume correction to γ_0, $\mu=\rho/\rho_0-1$, ρ is the density of water. When the fluid is in a negative pressure state, it can be expressed as:

$$P=\rho_0 C^2\mu+(\gamma_0+\alpha\mu)E^{'} \tag{7}$$

The material parameters of water are listed in Table 2. Moreover, the water was defined by the keyword "*MAT_NULL" and "*EOS_GRUNEISEN".

Table 2 Gruneisen equation of state parameters [28]

ρ (kg/m^3)	C (m/s)	S1	S2	S3	γ_0	α	E'/MPa
1025	1480	2.56	-1.986	0	0.49	0	0.2054

The state equation of air uses the polynomial equation state in this paper, which is given by Eq. (8):

$$P=c_0+c_1\mu+c_2\mu^2+c_3\mu^3+(c_4+c_5\mu+c_6\mu^2)\rho_0 E_0 \tag{8}$$

where the parameter P stands for the pressure, c_0-c_6 are constants, E_0 is the internal energy per initial volume. The corresponding parameters of air are given in Table 3.

Table 3 Parameters for air [8, 9, 30]

ρ (kg/m^3)	C_0	C_1	C_2	C_3	C_4	C_5	C_6	E_0
1.292	0	0	0	0	0.4	0.4	0	0.25

2.2.3 Plate model

Considering the influence of strain rate, the Cowper-Symonds (C-S) [31, 32] material model is used to simulate the material characteristics of the plate structure. The C-S material model is a relatively mature and widely used material model, which can consider strain hardening and strain rate effects in solving high-speed dynamic nonlinear problems such as impact, collision, and fracture of metal thin shells:

$$\sigma_Y=\left[1+\left(\frac{\dot{\varepsilon}}{Q}\right)^{\frac{1}{P}}\right]\sigma_0 \tag{9}$$

where $\dot{\varepsilon}$ is strain rate, Q and P are strain rate parameter, Q=40.4s^{-1}, P=5, σ_0 is initial yield stress. The material parameters of Q235 steel are shown in Table 4.

Table 4 The material parameters of Q235 steel [33]

ρ (kg/m^3)	G (MPa)	σ_0 (MPa)	Young's modulus (GPa)	Poisson's ratio	Rupture strain
7850	250	235	210	0.3	0.23

3. FEM calculation model underwater explosion

3.1 Finite element modelling

To accurately reproduce the damage characteristics of plate structures induced by the local effects of explosives under underwater explosion conditions and reveal the transient interaction mechanism between

them, this study establishes a three-dimensional (3D) coupled numerical model based on the theory of fluid-structure interaction (FSI) dynamics, which enables the quantitative analysis of the correlation mechanism between explosive loads and structural responses.

Considering that both the underwater explosion load and the plate structure exhibit geometric and physical symmetry—specifically, the explosive energy is uniformly distributed radially with the charge as the center, and the plate structure adopts a regular rectangular configuration with symmetric boundary constraints—a full-scale 3D model would lead to an exponential increase in the number of meshes and excessive consumption of computational resources. Therefore, a quarter-symmetric model was selected for simulation calculations. This modeling strategy significantly improves computational efficiency while ensuring computational accuracy and the fidelity of physical phenomena. The overall configuration of the model is shown in Fig. 1.

The overall computational domain size of the numerical model is 6m × 6m × 14m, which consists of three core components: the air domain, the water domain, and the plate structure. Specifically, the thickness of the air domain is set to 2m, serving to simulate the interface coupling effect between gas-phase and liquid-phase media during the underwater explosion process. The depth of the water domain is determined based on the actual layout position of the plate structure, which is fixed at a water depth of 6m. This configuration ensures that the plate structure is located in a typical effective region affected by underwater explosions, while avoiding the interference of shallow water effects on the propagation characteristics of shock waves. The plate structure is designed in a rectangular shape with a length and width of 1.4m each, which can cover the main influence range of the explosion effect. To investigate the sensitivity of the plate thickness parameter to the damage effect, four thickness gradients (2mm, 3mm, 4mm, and 5mm) are set to analyze the differences in damage modes under different structural stiffness conditions.

The boundaries of the plate structure are subjected to full fixed constraints, simulating the rigid connection state between the plate and surrounding structures in actual engineering to eliminate the interference of boundary displacement on local damage results. For the flow field (including the air domain and water domain), non-reflective boundary conditions are applied, which can effectively absorb the reflected energy of explosive shock waves at the boundaries of the computational domain. This avoids the disturbance of false reflected waves on the simulation results and ensures that the shock wave propagation and load action processes conform to actual physical laws. The central region of the numerical model adopts a dense mesh size with 0.05m, and the outer zone mesh size is 0.1m. The boundary of flow field is treated by non-reflective boundary.

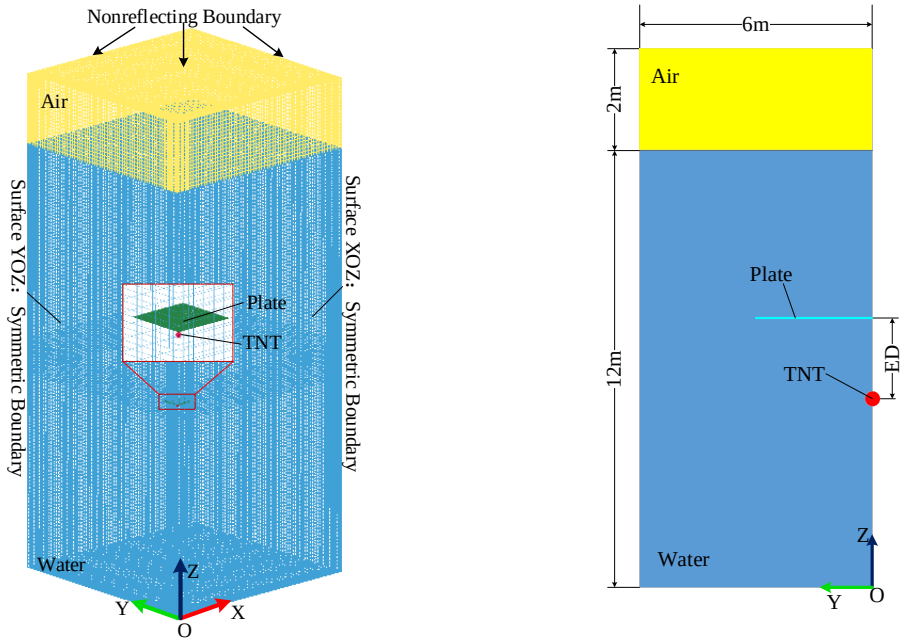

Fig. 1 Finite element modelling (a) Schematic diagram of numerical model, (b) Model size diagram (ED represents the distance from the charge centroid to the target plate)

To systematically investigate the influence law of explosive parameters on the local damage effect of plate structures, a variable combination scheme with multiple sets of charge mass and charge radius was designed. Specifically, the charge mass ranges from 23g to 853.5g, covering the energy interval of small to medium equivalent explosives, which can simulate the explosive action characteristics of underwater ammunitions with different powers.

Correspondingly, the charge radius ranges from 0.02m to 0.05m, increasing with an interval of 0.005m. This setting ensures the matching between the geometric size and mass parameters of the charge; meanwhile, through the gradient change of radius, the influence of charge morphology on the explosive energy release characteristics and shock wave load distribution law is analyzed.

Each set of charge parameters is collaboratively designed with the geometric characteristics and mesh generation scheme of the quarter-symmetric model, which guarantees the comparability of simulation conditions under different working conditions and lays a foundation for the subsequent construction of the "charge parameter-damage effect" correlation model.

3.2 Validation of the numerical method

The mesh size used in this study was determined with reference to References [8, 9] , and has undergone mesh convergence verification. The verification results are presented in Fig. 2. For the shock wave pressure time-history curve, the variation trends of the three meshes are basically consistent, with an inter-mesh error of approximately 6%. A further comparison between the peak pressures obtained under the three meshes and the Cole empirical formula reveals the following: when the mesh size is 0.025 m, the peak pressure is slightly larger than the value calculated by the Cole empirical formula, with an error of about 4.3%; when the mesh sizes are 0.05 m and 0.1 m, the peak pressures are both smaller than the values from the Cole empirical formula, with errors of approximately 5% and 6%, respectively. Considering both computational efficiency and accuracy requirements comprehensively, the 0.05 m mesh was ultimately selected, which can fully meet the needs of the current study.

In addition, the established numerical model was used to verify the bubble behavior of a 55 g charge, and the results are shown in Fig. 3. It can be seen from the figure that both the variation period and size of the bubble are basically consistent with the experimental results. When the maximum bubble radius obtained from the numerical simulation is compared with the experimental value, the error is only about 1.1%. It can thus be concluded that the constructed numerical model for bubbles is applicable to current research.

To ensure the reliability and accuracy of the numerical simulation results, a mesh independence verification analysis was conducted on the plate structure. The plate structure was modelled using shell elements, with the mesh size range set to 0.002–0.02 m and an interval of 0.004 m between adjacent mesh sizes. Meanwhile, to simulate actual working conditions, an underwater contact explosion load (with a charge mass of 10 g) was applied to the plate. A correlation curve between the mesh size and the plate’s breach diameter was obtained through calculations, and the specific results are shown in Fig. 4 (a). As indicated in Fig. 4 (a), when the mesh size of the plate is reduced to the critical threshold required for structural failure analysis, even if the mesh size of the plate is further reduced, the deviation amplitude between the maximum and minimum breach diameters of the plate induced by the explosion load remains less than 15%. This deviation level fully meets the error control requirements for numerical simulations in auxiliary research on underwater explosions.

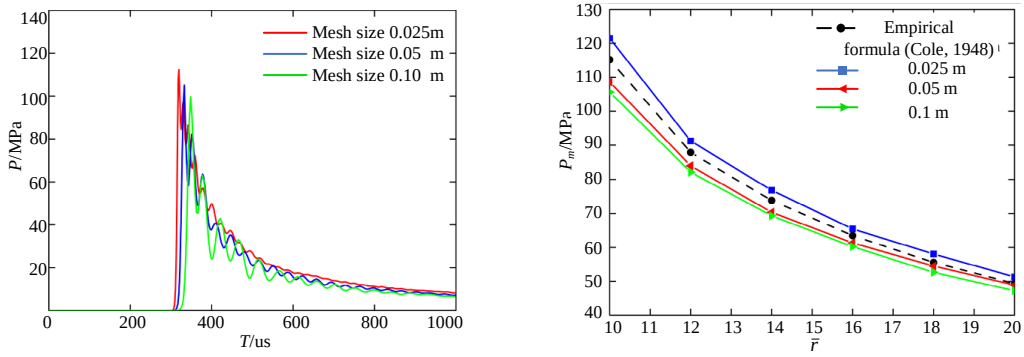

(a) (b)

Fig. 2 Shock pressures simulated by different mesh sizes [8], (a): Shock wave pressure versus time from three different element sizes at $\bar{r}$=10 ($\bar{r} = R_0 / R'$, R_0 is the explosion distance, R' is the radius of the charge); (b): The peak pressure of the shock wave at different $\bar{r}$

To verify the correctness of the numerical simulation results, a set of comparative experiments was carried out in this study. The steel plate structure used in the experiments had a length and width of 1.2 m each and a thickness of 2 mm (a mesh size of 0.01 m was used in the corresponding numerical simulation), with a charge mass of approximately 5.2 g. As shown in Figs. 4 (b) and (c): the actual breach size of the steel plate in the experiment was 19 mm, while the breach size predicted by the numerical simulation was approximately 22 mm, with a deviation of about 13.6% between the two. This deviation meets the accuracy requirements for underwater explosion research, indicating that this mesh parameter is suitable for numerical damage studies of plate-frame structures under underwater explosion loads.

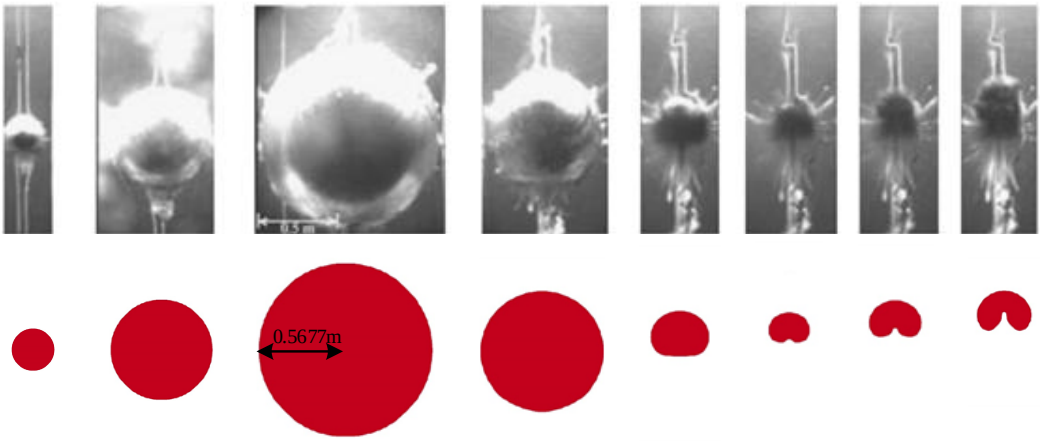

Fig. 3 The bubble shape of 55g TNT charge: from left to right, the bubble shape at t = 1, 7, 50, 85, 93, 94, 95, and 96 ms

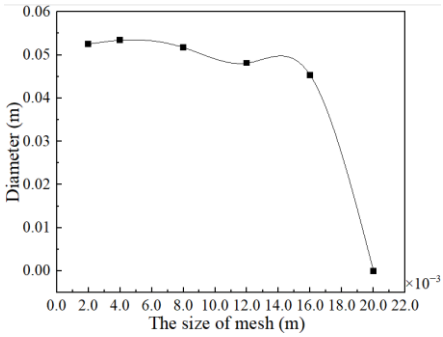

(a) Graph of the relationship between mesh size and crevasse diameter

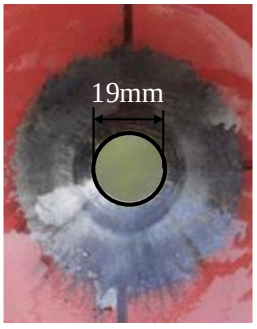

(b) Experimental result

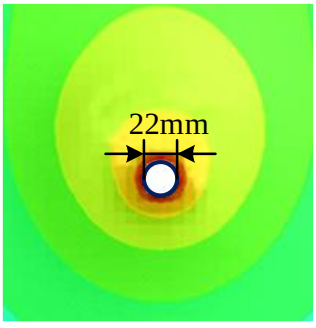

(c) Numerical simulation results

Fig. 4 Crevasse characteristics of the plate [34]

4. Numerical result

4.1 Analysis of damage characteristics of plate structure

Fig. 5 shows the damage cloud images of different plate thicknesses (2~5mm) under the working condition of 23g-15mm (Charge is 23g, explosion distance is 15mm, and the same below). As can be seen from the figure, the breach shape of the four types of thickness plates is all circular in this working condition, and the radius of the breach gradually decreases with the increase of the plate thickness. The damage radius of the plate with 2 mm~5 mm thickness is 73.23, 49.43, 38.56, 34.38 mm, respectively. At the same time, the plastic deformation range of the plate increases with the increase of plate thickness.

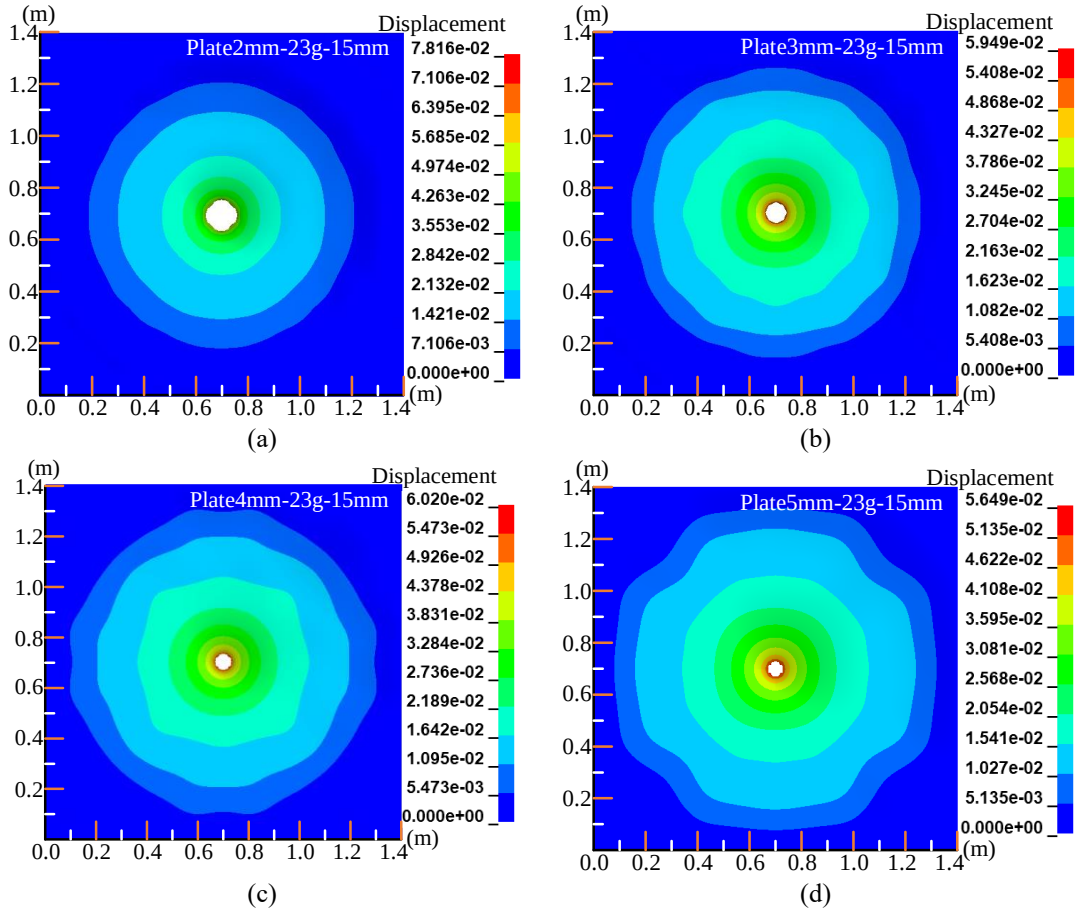

Fig. 5 Damage cloud image of different plate thickness under 23g-15mm working condition, (a) The thickness of the plate is 2 mm, (b) The thickness of the plate is 3 mm, (c) The thickness of the plate is 4 mm, (d) The thickness of the plate is 5mm

Fig. 6 shows the damage cloud images of plates with different thicknesses (2~5 mm) under the working condition of 55g-20mm. It can be seen from the figure that when the plate thickness is 2 mm and 3 mm, the breach shape is gear-like; in contrast, the breach shape of the 4 mm-thick and 5 mm-thick plates is quadrilateral. With the increase in plate thickness, the breach radius decreases while the plastic deformation area increases. The damage radii of the plates with thicknesses of 2 mm, 3 mm, 4 mm, and 5 mm are 111.87 mm, 81.91 mm, 66.99 mm, and 53.92 mm, respectively.

Fig. 7 displays the damage cloud images of plates with different thicknesses (2~5 mm) under the working condition of 106g-25mm. As can be observed from the figure, when the plate thickness is 2 mm, the breach shape is rectangular; when the plate thickness is 3 mm, the breach shape is gear-like; and when the plate thickness is 4 mm and 5 mm, the breach shape is cross-teared rectangular. Additionally, with the increase in plate thickness, the breach radius decreases gradually (the damage radii of the plates with thicknesses of 2 mm, 3 mm, 4 mm, and 5 mm are 178.48 mm, 107.87 mm, 95.63 mm, and 93.42 mm, respectively), while the plastic deformation area expands gradually.

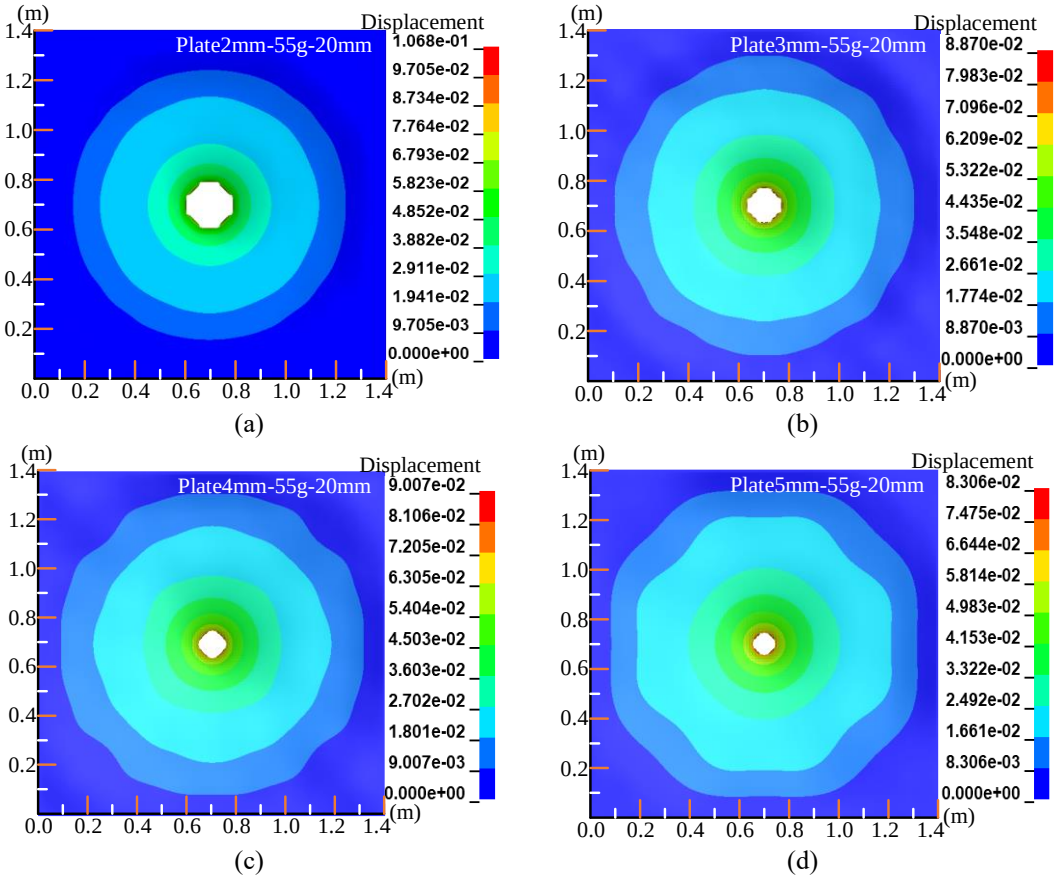

Fig. 6 Damage cloud image of different plate thickness under 55g-20mm working condition, (a) The thickness of the plate is 2 mm, (b) The thickness of the plate is 3 mm, (c) The thickness of the plate is 4 mm, (d) The thickness of the plate is 5mm

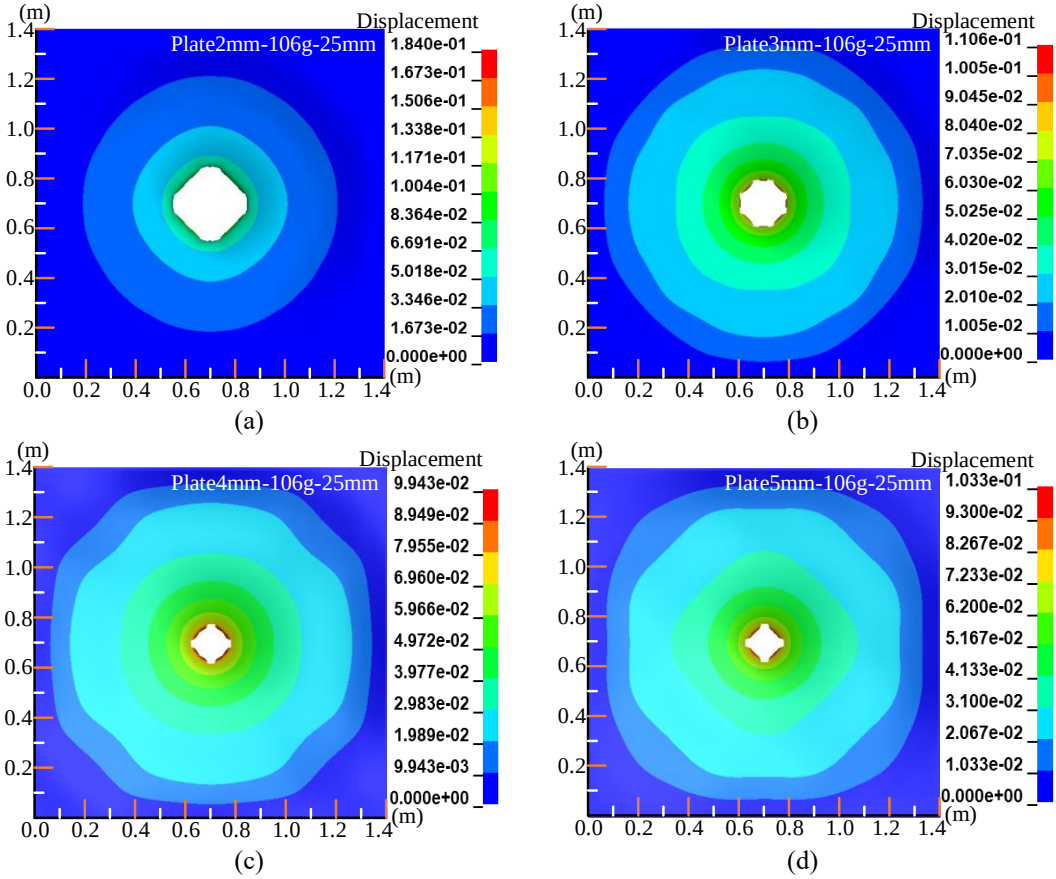

Fig. 7 Damage cloud image of different plate thickness under 106g-25mm working condition, (a) The thickness of the plate is 2 mm, (b) The thickness of the plate is 3 mm, (c) The thickness of the plate is 4 mm, (d) The thickness of the plate is 5mm

Fig. 8 presents the damage cloud images of plates with different thicknesses (2~5 mm) under the working condition of 185g-30mm. As can be seen from the figure, when the plate thickness ranges from 2 mm to 4 mm, the breach shape is rectangular; when the plate thickness is 5 mm, the breach shape is cross-teared rectangular. Moreover, with the increase in plate thickness, the breach radius decreases gradually (the damage radii of the plates with thicknesses of 2 mm, 3 mm, 4 mm, and 5 mm are 227.12 mm, 176.64 mm, 155.05 mm, and 130.92 mm, respectively), while the plastic deformation area expands gradually.

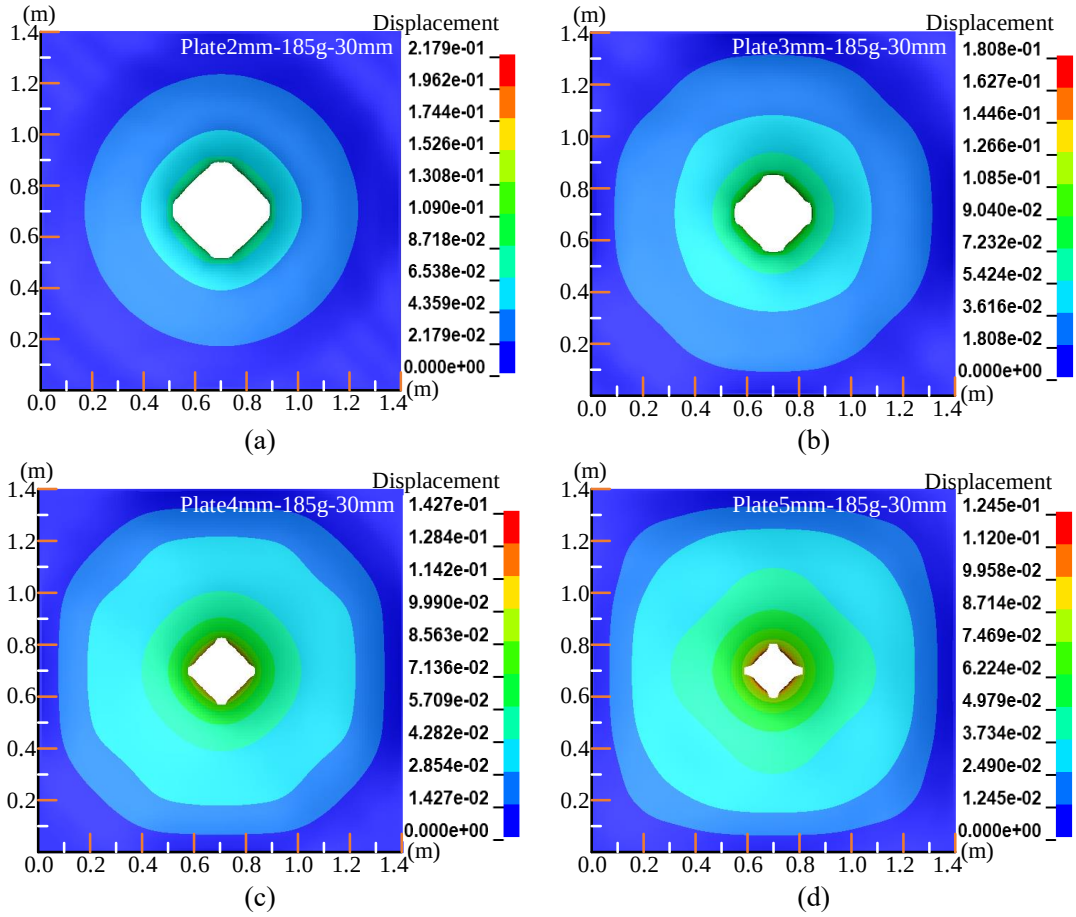

Fig. 8 Damage cloud image of different plate thickness under 185g-30mm working condition, (a) The thickness of the plate is 2 mm, (b) The thickness of the plate is 3 mm, (c) The thickness of the plate is 4 mm, (d) The thickness of the plate is 5mm

From the aforementioned analysis, the following key conclusions can be drawn: with an increase in plate thickness, the breach radius decreases progressively, while the plastic deformation area expands gradually.

Mechanistically, a greater plate thickness corresponds to higher structural strength and enhanced resistance to tearing and shearing. This elevated mechanical performance effectively suppresses the initiation and propagation of fractures induced by underwater explosion loads, thereby resulting in a reduced breach radius. Concurrently, a smaller breach leads to a diminished load unloading area i.e., the region through which the explosive load is dissipated via the breach is narrowed. This narrowing effect extends the spatial range of shock wave action on the plate; over time, the damage to the plate propagates from the central load-applied region toward the boundary rather than being concentrated solely in the central area. Collectively, these two effects synergistically drive the observed trends: as plate thickness increases, the breach radius decreases monotonically, and the extent of the plastic deformation region expands progressively.

Additionally, the breach radius is positively correlated with charge mass an increase in charge mass leads to a larger breach radius. This correlation stems from the fact that a larger charge releases greater explosive energy, which generates a more intense shock wave. The enhanced shock wave imparts a higher impulse to the plate surface, more effectively overcoming the plate's mechanical resistance and promoting the radial expansion of fractures, thereby resulting in an increased breach radius.

To intuitively analyze the influence of ammunition local effects on the inherent local damage mechanism of target structures and eliminate interference from structural dimensions, the fracture characteristics of the plate structure and corresponding explosion conditions were subjected to dimensionalization. Based on the results of numerical experiments, the mathematical relationship between the structural dimensionless factor and the explosive impact factor was derived and constructed. Considering that the loading range of shock waves acting on the structure under contact explosion is determined by the explosive's projected area, the impact factor selected in this study is defined as follows: $\sqrt{W}/R'$ (W is the charge, R' is the radius of the charge). To eliminate the influence of plate size on the evaluation of fracture characteristics, the structural dimensionless factor is defined as R/L (R represents the radius of the crevasse and L represents the side length of the plate).

As observed from Figs. 9 (a) to (d), regardless of the plate thickness (2 mm, 3 mm, 4 mm, or 5 mm), the ratio of the breach radius to the plate's side length (R/L) increases with the growth of the impact factor ($\sqrt{W}/R'$). Meanwhile, curve fitting was performed on the data, and corresponding fitting equations were established. To improve fitting accuracy, a third-order fitting was initially conducted for the curves in this study. However, a comparison of the fitting coefficients revealed that the third-order coefficients were relatively small and thus negligible. Therefore, each curve can be represented by a quadratic equation with sufficient precision.

This quadratic equation enables the prediction of fracture behaviors for other plates under contact explosion conditions, providing convenience for investigating the structural damage characteristics induced by contact explosions.

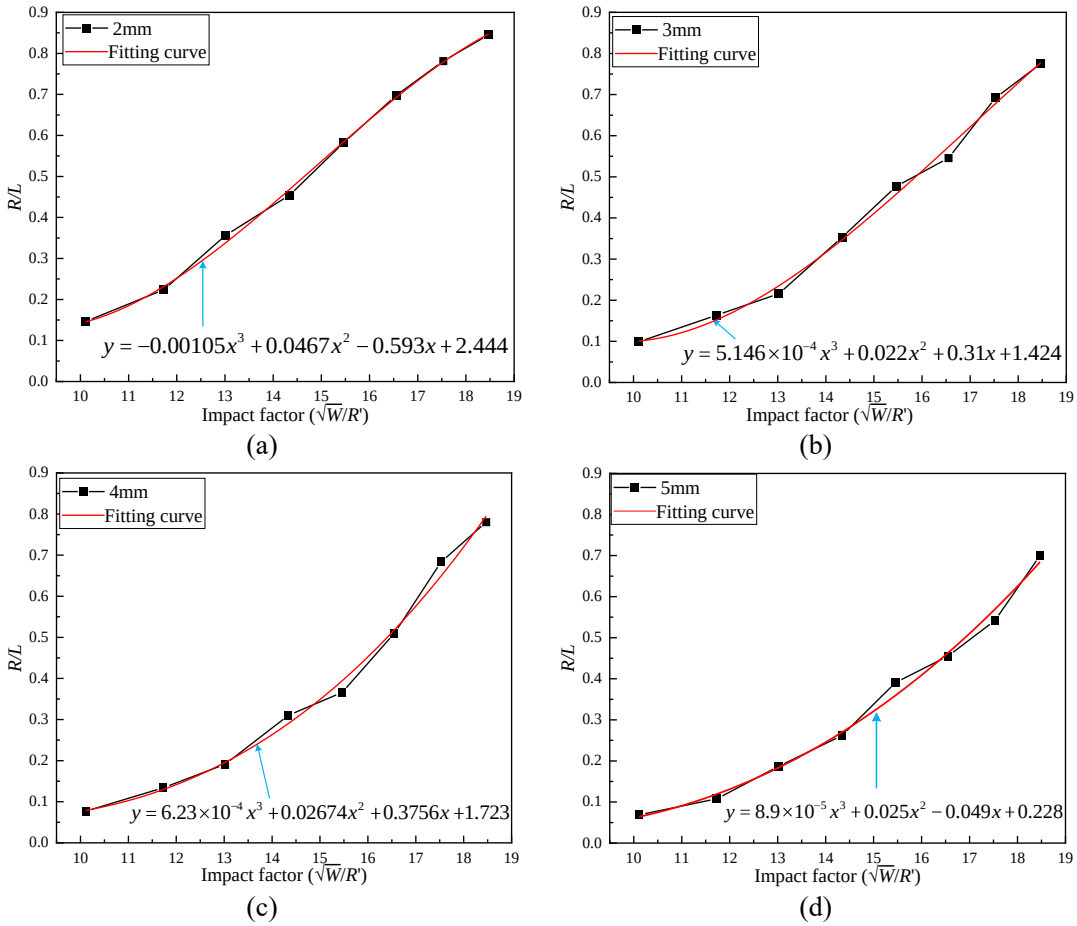

Fig. 9 The relationship between breach radius and impact factor ($\sqrt{W}/R'$)

4.2 Damage analysis of plate structure by local damage effect of explosive

In the process of underwater contact explosion, the plate structure is not only affected by shock wave loads but also subjected to damage induced by the detonation high temperature (including deflagration

temperature and initiation temperature) generated during the explosion. In extreme cases, this high temperature can cause ablation and perforation of the plate structure, forming holes. Meanwhile, the accompanying impact load will further tear and expand the holes, exacerbating structural damage.

With the increase of explosion distance, the destructive effect of the explosion-induced high temperature on the structure gradually diminishes; however, the impact load still causes damage to the plate-frame structure, which may lead to tearing or even shear failure under severe conditions. Regardless of whether the structural damage is caused by impact load or ablation, the detonation products generated by the explosion will penetrate through the damaged area to the backside of the plate, enabling partial unloading of the impact load.

Subsequently, as the standoff distance increases, the wavefront area expands accordingly, resulting in a decrease in peak pressure [35], consequently, the destructive effect of the load on the structure is weakened.

Taking an 853.5 g charge as an example, the damage morphologies of the plate under different explosion distances are presented in Fig. 10. As the explosion distance increases, the breach shape of the plate evolves sequentially as circular, octagonal, rectangular, and lotus-petal-like. In this study, the maximum tear length was defined as the breach radius; a summary analysis of the breach radii under different working conditions was conducted, with the results shown in Fig. 11.

Fig. 11. illustrates the relationship between the plate's breach radius and explosion distance under various working conditions. It can be observed from the figure that when the charge mass is small (12 g and 55 g), the breach radius induced by the explosion on the plate structure (with thicknesses of 2 mm, 3 mm, 4 mm, and 5 mm) decreases with the increase of explosion distance. However, as the charge mass increases, the relationship between the breach radius of the steel plate structure and the explosion distance no longer follows the trend of decreasing with increasing explosion distance.

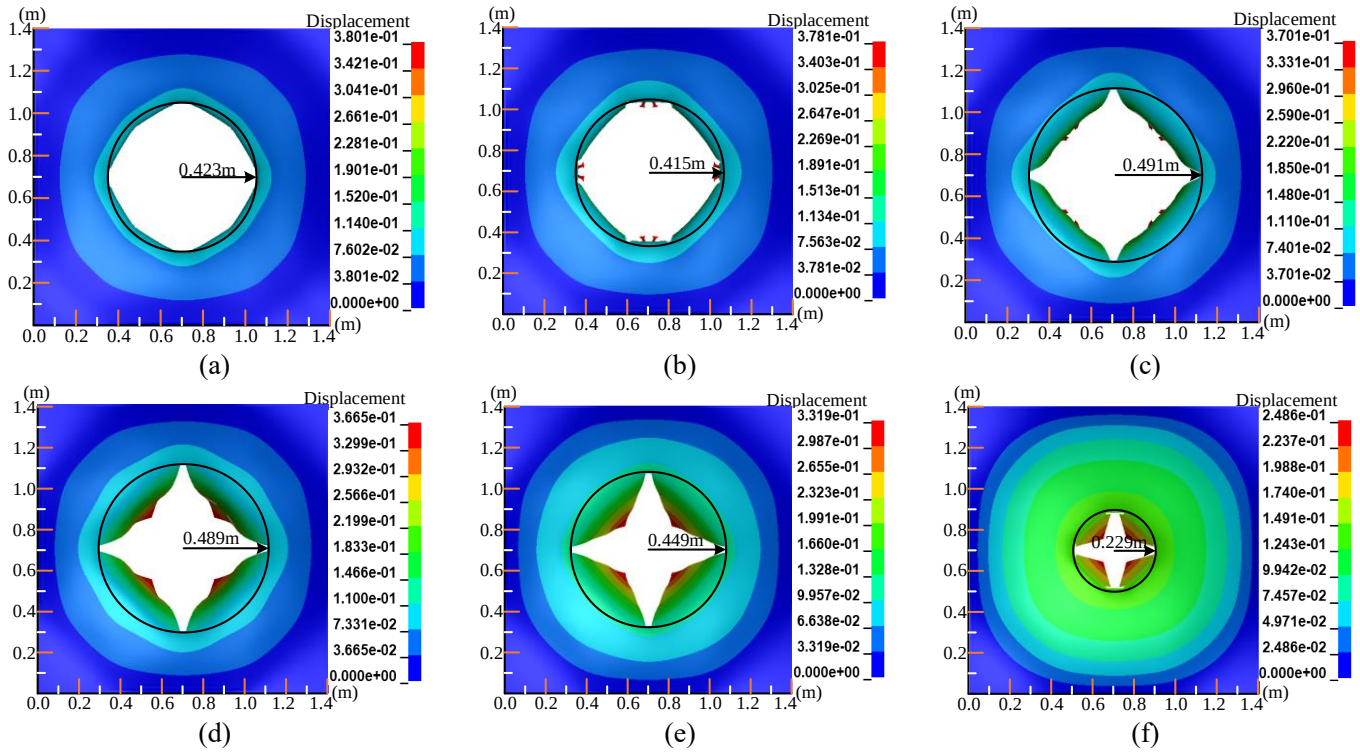

Fig. 10 Damage cloud of 853.5g charge with different explosion distance, the explosion distances of (a) to (f) are 50mm, 70mm, 90mm, 110mm, 130mm and 150mm respectively

As shown in Fig. 11 (a), when the plate thickness is 2 mm and the charge mass ranges from 185 g to 853.5 g, the breach radius first decreases, then increases, and finally decreases with the increase of explosion distance. This phenomenon is attributed to the local effect of the explosive. Specifically, when the explosion distance is small, the high temperature generated by the explosion causes ablation on the plate; this high-temperature ablation induces a small range of cracks on the plate, with a size approximately equal to the

ammunition diameter. Subsequently, the high-pressure gas (bubbles) produced by the explosion penetrates through the breach to the backside of the plate (the side opposite to the explosion), enabling partial unloading of the impact load. As the explosion distance increases, the influence of the explosion-induced high temperature on the plate gradually diminishes, and the peak pressure of the shock wave also decreases gradually during the unloading process.

Consequently, the breach radius decreases initially. With the continuous increase of explosion distance, when the explosion-induced high temperature no longer affects the plate, the shock wave load is fully applied to the plate. Meanwhile, the loading range of the shock wave is much larger than the ablation range caused by high temperature on the plate; thus, the breach radius of the plate increases. After that, as the explosion distance continues to increase, the peak pressure of the load decreases, leading to a subsequent decrease in the breach radius. In the context of structural impact damage induced by underwater explosions, the phenomenon wherein the structural damage effect first diminishes and subsequently intensifies (exceeding the severity of prior damage) with increasing explosion distance is defined as the localized damage effect of explosive.

Similarly, when the plate thicknesses are 3 mm and 4 mm, the local effect of the explosive emerges when the charge mass reaches 292.6 g, as illustrated in Figs. 11 (b) and (c); when the plate thickness is 5 mm, the local effect of the explosive appears when the charge mass reaches 438 g, as shown in Fig. 11 (d).

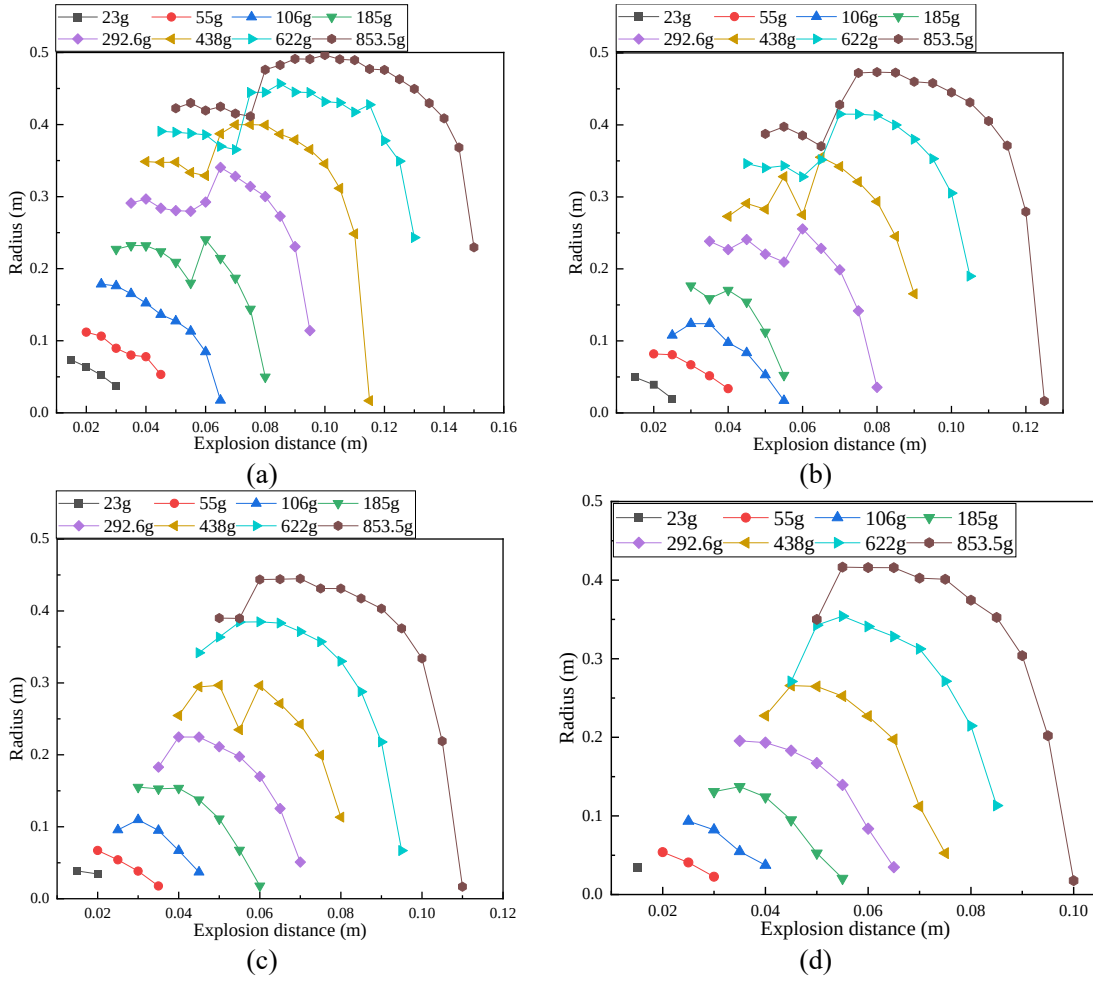

Fig. 11 Diagram of breach radius and explosion distance of plate, (a), (b), (c) and (d) represent plate thickness of 2mm, 3mm, 4mm and 5mm respectively

The above working conditions are dimensionless, as shown in Eq. (10):

$$\bar{r} = \frac{R_0}{R'} \tag{10}$$

where, $\bar{r}$ is relative explosion distances, R_0 is the distance from the explosion center to the plate, R' is the radius of charge. The relative explosion distances of the plates with the maximum crevasse under different working conditions are summarized.as show from Table 5. With the increase of plate thickness, the relative explosion distance decreases, and the influence of local effect of explosive on plate decreases gradually.

Table 5 Summary of relative explosion distance at maximum crevasse under different conditions

Case	185g	292.6g	438g	622g	853.5g
2mm	2	1.889	1.875	1.889	2
3mm	-	1.714	1.625	1.556	1.5
4mm	-	1.143	1.25	1.333	1.2
5mm	-	-	1.125	1.222	1.1

From the aforementioned analysis, it can be concluded that the local effect of ammunition is induced by contact explosion. Specifically, the high-temperature range generated by the explosion is capable of affecting the plate structure, and the energy released by the ammunition can achieve the effect of instantly inducing ablative damage to the plate.

Notably, the local effect of ammunition is most pronounced when the relative explosion distance falls within the range of 1.1–2. Within this range, the destructive capacity of the underwater explosion reaches its maximum, this is attributed to the optimal superimposition of the explosion-induced high-temperature ablation effect and the shock wave load effect: the high temperature is sufficient to induce initial cracks on the plate, while the shock wave load can effectively expand these cracks, thereby maximizing the structural damage.

In addition, the local effect of the explosive is correlated with the plate thickness: the thinner the plate, the more pronounced the local effect; conversely, the thicker the plate, the less obvious the local effect, or even no local effect occurs.

Meanwhile, when the plate structure is subjected solely to load (i.e., without the influence of explosion-induced high temperature), the breach size of the plate decreases correspondingly as the shock wave intensity diminishes.

5. Conclusion

In this study, numerical impact experiments of underwater explosions on plate structures were conducted under varying charge masses and explosion distances, aiming to investigate the local damage effect of explosives. Through the analysis of numerical results, the key conclusions are drawn as follows:

1. For contact underwater explosions, the breach shapes of steel plate structures can be essentially categorized into four types: circular, gear-like, rectangular, and cross-teared. These shape variations are primarily driven by the combined effects of charge mass, explosion distance, and plate thickness, reflecting the different stress distribution patterns and fracture propagation modes induced by explosive loads.

2. On the premise that the charge mass is sufficient to induce breaches on the plate, fitting analysis was performed to explore the relationship between the impact factor and the structural dimensionless factor. The results indicate a quadratic functional relationship between these two factors. This quadratic formula exhibits universality for the damage assessment of bare plate structures under underwater explosions, providing a reliable reference for predicting the structural damage induced by other charge masses under contact explosion conditions.

3. The local effect of underwater explosions is correlated with the structural strength of the plate. Under underwater contact explosion, when the detonation high temperature induces ablative breaches on the structure, the continuous expansion of these breaches increases the load unloading area. Consequently, the plastic deformation area caused by the shock wave load on the structure decreases. In contrast, when the load is fully applied to the structure (i.e., no ablative breaches to facilitate unloading), the destructive effect of the explosive load on the structure is enhanced. This finding not only offers guidance for optimizing the efficiency of underwater blasting operations but also provides a theoretical reference for the anti-explosion design of marine structures and the interception of underwater weapons.

4. For steel plate structures, with the attenuation of plate thickness, the significance of the local effect of underwater explosions gradually increases. If it is necessary to achieve the strongest destructive effect of underwater explosions on steel plate structures, combined with the aforementioned analysis results, it is recommended to control the relative explosion distance within the range of 1.1–2.

6. Acknowledgements

The authors would like to thank the support from the General Project of Scientific Research Program of Hunan Provincial Department of Education (24C0285) and National Natural Science Foundation of China (12172100).

REFERENCES

[1] Chung, J., Seo, Y., Shin, Y.S., 2020. Dynamic and whipping response of the surface ship subjected to underwater explosion: experiment and simulation. *Ships and Offshore Structures*, 15(10), 1129-1140. https://doi.org/10.1080/17445302.2019.1706924

[2] Zong, Z., Zhao, Y.J., Li, H.T., 2013. A numerical study of whole ship structural damage resulting from close-in underwater explosion shock. *Marine Structures*, 31, 24-43. https://doi.org/10.1016/j.marstruc.2013.01.004

[3] Sun, W., Zhu, T., Chen, P., Lin, G., 2022. Dynamic implosion of submerged cylindrical shell under the combined hydrostatic and shock loading. *Thin-Walled Structures*, 170. https://doi.org/10.1016/j.tws.2021.108574

[4] Zhang, S.R., Wang, G.H., Wang, C., Pang, B.H., Du, C.B., 2014. Numerical simulation of failure modes of concrete gravity dams subjected to underwater explosion. *Engineering Failure Analysis*, 36, 49-64. https://doi.org/10.1016/j.engfailanal.2013.10.001

[5] Zhang, Q.L., Li, D.Y., Wang, F., Li, B., 2018. Numerical simulation of nonlinear structural responses of an arch dam to an underwater explosion. *Engineering Failure Analysis*, 91, 72-91. https://doi.org/10.1016/j.engfailanal.2018.04.025

[6] Orlov, M., 2019. Investigation of the process of explosive loading of freshwater ice. *Thermal Science*, 23(Suppl. 2), 561-567. https://doi.org/10.2298/TSCI19S2561O

[7] Wang, Q., Wang, Y., Zan, Y.F., Lu, W.B., Bai, X.L., Guo, J., 2017. Peridynamics simulation of the fragmentation of ice cover by blast loads of an underwater explosion. *Journal of Marine Science and Technology*, 23(1), 52-66. https://doi.org/10.1007/s00773-017-0454-x

[8] Wang, Y., Qin, Y.Z., Yao, X.L., 2020. A combined experimental and numerical investigation on damage characteristics of ice sheet subjected to underwater explosion load. *Applied Ocean Research*, 103, 102347. https://doi.org/10.1016/j.apor.2020.102347

[9] Wang, Y., Qin, Y.Z., Wang, Z.K., Yao, X.L., 2021. Numerical study on ice damage characteristics under single explosive and combination explosives. *Ocean Engineering*, 223, 108688. https://doi.org/10.1016/j.oceaneng.2021.108688

[10] Wang, Z., Yang, S., Yang, L., Xu, W., Dong, Y., Li, D., Qu, J., Wu, L., 2026. Experimental and numerical studies on the effect of sandwich structures on the dynamic response of ship sections subjected to underwater explosions. *Thin-Walled Structures*, 218, 113969. https://doi.org/10.1016/j.tws.2025.113969

[11] He, Z., Du, Z., Zhang, L., Li, Y., 2023. Damage mechanisms of full-scale ship under near-field underwater explosion. *Thin-Walled Structures*, 189, 110872. https://doi.org/10.1016/j.tws.2023.110872

[12] He, Z., Chen, X., Zhang, X., Jiang, Y., Ren, X., Li Y., 2025. Damage prediction of hull structure under near-field underwater explosion based on machine learning. *Applied Ocean Research*, 154, 104329. https://doi.org/10.1016/j.apor.2024.104329

[13] Madsen, B., Morgan, G., Rousseau, C.-E., Shukla, A., 2024. Performance of flat-plate aluminum structures subjected to in-contact underwater explosions. *Journal of Fluids and Structures*, 125, 104084 https://doi.org/10.1016/j.jfluidstructs.2024.104084

[14] Cheng, L., Huang, F., Wu, H., Dong, H., Tian, S., 2024. Cumulative damage effects of repeated underwater explosions on multi-cabin structures. *Thin-Walled Structures*, 204, 112231. https://doi.org/10.1016/j.tws.2024.112231

[15] Shi, D., Wang, J., Wang, Z., Wasim, M.K.H., 2024. Nonlinear similarity characterisation and validation of dynamic response of ship stiffened plate structure under explosion load impacts. *Scientific Reports*, 14(1), 15804. https://doi.org/10.1038/s41598-024-66366-6

[16] Yao, X., Zhao, K., Shi, D., 2024. Study on the effectiveness of impact factor in underwater explosion model test. *International Journal of Impact Engineering*, 185, 104839. https://doi.org/10.1016/j.ijimpeng.2023.104839

[17] Yao, X., Yin, Y., Zhao, K., Huang, R., 2025. A study of diffeomorphism characterization in similar transformation of underwater explosion ship model tests. *Nonlinear Dynamics*, 113, 31009-31038. https://doi.org/10.1007/s11071-025-11676-1

[18] Lee, S., Cho, J., Lee, C., Cho, S., 2021. Experimental and numerical investigations of near-field underwater explosions. *Structural Engineering and Mechanics*, 77(3), 395-406.

[19] Cheng, L., Huang, F., Wu, H., Dong, H., Tian, S., 2024. Comparative analysis of blast load transfer and structural damage in multi-cabin structures during air and underwater explosions. *Ocean Engineering*, 297, 116953. https://doi.org/10.1016/j.oceaneng.2024.116953

[20] Lin, S., Wang, J., Tang, K., Yang, M., Ma, T., Gu, Y., Li, Y., 2025. Investigation of damage effects on circular air-backed clamped plates under repeated underwater explosions. *Ships and Offshore Structures*, 1-15. https://doi.org/10.1080/17445302.2025.2452057

[21] Wei, Y., Zhang, J., Liu, K., Pan, J., Zhang, L., Chen, W., Zhang, Q., 2025. Numerical study of the influence of hydrofoil hydrodynamic performance considering near-free surface. *Brodogradnja*, 76(1), 76108. https://doi.org/10.21278/brod76108

[22] Bal, K., Bayraktar Bural, D., 2024. Investigation into forces on offshore piles with constant and linearly varying diameters using CFD and extended Morison equation under separate wave and current loadings. *Brodogradnja*, 75(4), 75406. https://doi.org/10.21278/brod75406

[23] Wang, M., Qiao, D., Zhou, X., Tang, G., Lu, L., Ou, J., 2024. Dynamic responses analysis of submerged floating tunnel under impact load. *Brodogradnja*, 75(2), 75208. http://dx.doi.org/10.21278/brod75208

[24] Kim, J.H., Shin, H.C., 2008. Application of the ALE technique for underwater explosion analysis of a submarine liquefied oxygen tank. *Ocean Engineering*, 35(8-9), 812-822. https://doi.org/10.1016/j.oceaneng.2008.01.019

[25] Tai, Y.S., Chu, T.L., Hu, H.T., Wu, J.Y., 2011. Dynamic response of a reinforced concrete slab subjected to air blast load. *Theoretical and Applied Fracture Mechanics*, 56(3), 140-147. https://doi.org/10.1016/j.tafmec.2011.11.002

[26] Donea, J., 1983. Arbitrary Lagrangian-Eulerian finite element methods [DS]. Computational Methods for Transient Analysis, Chapter 14.

[27] Marsh, S.P., 1980. LASL shock Hugoniot Date [M]. Berkeley: University of California Press.

[28] Praba, R.P.S., Ramajeyathilagam, K., 2020. Numerical investigations on the large deformation behaviour of ring stiffened cylindrical shell subjected to underwater explosion. *Applied Ocean Research*, 101, 102262. https://doi.org/10.1016/j.apor.2020.102262

[29] LS-DYNA theory Manual, 2017. Livermore Software Technology Corporation (LSTC).

[30] Song, G., Chen, Z.Y., Long, Y., Zhong, M.S., Wu, J.Y., 2017. Experimental and numerical investigation of the centrifugal model for underwater explosion shock wave and bubble pulsation. *Ocean Engineering*, 142, 523-531. https://doi.org/10.1016/j.oceaneng.2017.04.035

[31] Cowper, G.R., Symonds P.S., 1957. Strain-hardening and strain-rate effects in the impact loading of cantilever beams Providence [R]. USA: Division of applied mathematics, Brown University. https://doi.org/10.21236/AD0144762

[32] Suresh, C., Ramajeyathilagam, K., 2021. Large Deformation Behaviour of Thin Mild Steel Rectangular Plates Subjected to Underwater Explosion Loading under Air and Water Backed Conditions. *Applied Ocean Research*, 114, 102780. https://doi.org/10.1016/j.apor.2021.102780

[33] Qin, Y.Z., Wang, Y., Wang, Z.K., Yao, X.L., 2021. Damage characteristics of fixed single-layer squaresteel plate under near-field underwater explosion of small equivalent column charge. *Journal of Vibration and Shock*, 40(7), 29-36.

[34] Ming, F.R., Zhang, A.M., Xue, Y.Z., Wang, S.P., 2016. Damage characteristics of ship structures subjected to shockwaves of underwater contact explosions. *Ocean Engineering*, 117, 359-382. https://doi.org/10.1016/j.oceaneng.2016.03.040

[35] Cole, R.H., Weller, R., 1948. Underwater Explosions. *Physics Today*, 1(6), 35-36. https://doi.org/10.1063/1.3066176